Published in final edited form as:
J Lipid Res. 2006 April ; 47(4): 745–754. doi:10.1194/jlr.M500553-JLR200.

Agpat6 deficiency causes subdermal lipodystrophy and resistance to obesity[S]

Laurent Vergnes[*], **Anne P. Beigneux**[†], **Ryan Davis**[§], **Steven M. Watkins**[§], **Stephen G. Young**[†], and **Karen Reue**[1,*]

[*]Departments of Medicine and Human Genetics, David Geffen School of Medicine, University of California, Los Angeles, CA 90095, and VA Greater Los Angeles Healthcare System, Los Angeles, CA 90073

[†]Division of Cardiology, Department of Internal Medicine, University of California, Los Angeles, CA 90095

[§]Lipomics Technologies, West Sacramento, CA 95691

Abstract

Triglyceride synthesis in most mammalian tissues involves the sequential addition of fatty acids to a glycerol backbone, with unique enzymes required to catalyze each acylation step. Acylation at the *sn*-2 position requires 1-acylglycerol-3-phosphate *O*-acyltransferase (AGPAT) activity. To date, seven *Agpat* genes have been identified based on activity and/or sequence similarity, but their physiological functions have not been well established. We have generated a mouse model deficient in AGPAT6, which is normally expressed at high levels in brown adipose tissue (BAT), white adipose tissue (WAT), and liver. *Agpat6*-deficient mice exhibit a 25% reduction in body weight and resistance to both diet-induced and genetically induced obesity. The reduced body weight is associated with increased energy expenditure, reduced triglyceride accumulation in BAT and WAT, reduced white adipocyte size, and lack of adipose tissue in the subdermal region. In addition, the fatty acid composition of triacylglycerol, diacylglycerol, and phospholipid is altered, with proportionally greater polyunsaturated fatty acids at the expense of monounsaturated fatty acids. Thus, *Agpat6* plays a unique role in determining triglyceride content and composition in adipose tissue and liver that cannot be compensated by other members of the *Agpat* family.

Supplementary key words

acyltransferase; gene-trap; adipose tissue; energy expenditure; 1-acylglycerol-3-phosphate *O*-acyltransferase

Triglycerides are the primary form of energy storage in mammals, and alterations in triglyceride biosynthesis and metabolism can lead to metabolic diseases such as hyperlipidemia, obesity, and lipodystrophy. In eukaryotes, two major pathways exist for triglyceride synthesis: the glycerol phosphate pathway and the monoacylglycerol pathway. The monoacylglycerol pathway functions predominantly in small intestine to generate triglycerides from monoacylglycerol in dietary fat. The glycerol phosphate pathway, in contrast, is considered

[S]The online version of this article (available at http://www.jlr.org) contains additional table and figure.

[1]To whom correspondence should be addressed. reuek@ucla.edu.

Supplemental Material can be found at: http://www.jlr.org/cgi/content/full/M500553-JLR200/DC1

the main pathway for triglyceride synthesis and occurs in most cells types. In particular, it is responsible for triglyceride synthesis in adipose tissue. Acylation of glycerol phosphate occurs through a step-wise addition of acyl groups, each addition being catalyzed by a distinct enzyme (1,2). In recent years, the cloning and identification of several of these enzymes has facilitated their molecular characterization, but many questions remain about the physiological functions of these enzymes.

To date, only a few mouse models with genetic deficiency in the triglyceride biosynthetic pathway have been reported. Mice lacking the mitochondrial glycerol-3-phosphate acyltransferase (GPAT), which catalyzes the addition of the first acyl group to glycerol-3-phosphate, showed reduced levels of triglycerides in plasma and liver (3). They also had reduced body weight and adipose tissue mass. Deficiency in acyl-coenzyme A:diacylglycerol acyltransferase-1 (DGAT1), responsible for the final step in triglyceride synthesis, leads to reduced adiposity and resistance to diet-induced obesity (4). *Dgat1*-deficient (*Dgat1*$^{-/-}$) mice also showed increased energy expenditure, attributable in part to increased locomotor activity and increased levels of uncoupling protein-1, insulin, and leptin (4–6). Interestingly, *Dgat1*$^{-/-}$ mice had dry fur and hair loss, which were associated with atrophic sebaceous glands and abnormal lipid composition in the fur (7). Mice deficient in DGAT2 had a marked reduction in triglyceride synthesis and died at birth (8). These studies demonstrated that DGAT2 is essential for viability and that DGAT1 is unable to compensate for a deficiency in DGAT2.

Although GPATs and DGATS catalyze the initial and final acylation steps in triglyceride synthesis from glycerol phosphate, the 1-acylglycerol-3-phosphate *O*-acyltransferase (AGPAT) enzymes act at an intermediate step. The product of the GPAT reaction, lysophosphatidic acid, is again acylated, this time by an AGPAT, to form phosphatidic acid (1,2). Several AGPAT proteins have been reported and designated AGPAT1 through AGPAT7. An eighth related sequence was identified recently and designated AGPAT8 (accession number NP_766303; (9)). AGPAT1 and AGPAT2 are well characterized, and their enzymatic activity has been documented (10,11), whereas the other AGPAT family members were identified based upon sequence homology (12–14) or very modest activity levels (15). Mutations in *Agpat2* have been reported in patients with congenital generalized lipodystrophy (16,17), but no genetically modified animal model of any member of the AGPAT family has been generated. To investigate the importance of AGPAT enzymes in triglyceride biosynthesis and metabolism, we created and characterized a mouse model deficient in one of the most recently described family members, AGPAT6 (previously designated LPAAT-ζ) (13). We identified the mouse *Agpat6* gene from sequence tags within the BayGenomics database. We used *Agpat6* knockout embryonic stem cells to produce *Agpat6*$^{-/-}$ mice and then characterized the physiological role of this enzyme in adipose tissue and lipid metabolism.

MATERIALS AND METHODS

Generation of *Agpat6*$^{-/-}$ mice

Mouse embryonic stem cells containing a gene-trap insertion in the *Agpat6* gene (cell line number DTM030) were obtained from the BayGenomics gene-trap consortium (baygenomics.ucsf.edu) (18). The insertion of the gene-trap into the *Agpat6* gene was verified by direct sequencing of an ES cell cDNA obtained by 5′ rapid amplification of cDNA ends. Chimeric mice were generated by blastocyst injection and bred to C57BL/6J mice to establish lines carrying the insertional mutation in *Agapt6*. Offspring were genotyped by PCR with primers specific for the wild-type *Agpat6* allele (*Agpat*6-F, ggattcaagcactcggcagtc; *Agpat*6-R, gctctacgagaggcaagagg) and for *lacZ* in the gene-trap allele (*LacZ*-F, actggcagatgcacggttacg; *LacZ*-R, cgtagtgtgacgcgatcggca). The combination of the two primer sets made it possible to distinguish mice homozygous for the wild-type allele, heterozygous mice, and mice homozygous for the mutant allele. All blood and tissue samples were obtained after an

overnight (16 h) fast. Mice were anesthetized with isoflurane gas. Plasma was stored with EDTA at −80°C. Tissues were dissected, snap-frozen in liquid nitrogen, and stored at −80°C.

Body weight studies

To minimize the number of mice used, weight curves were generated from male mice fed a standard laboratory chow diet (Purina 5001) and from female mice fed a high-fat/high-carbohydrate (HF/HC) diet (Diet F3282; Bioserve, Frenchtown, NJ). A limited number of female mice were also studied on the chow diet and showed similar results as males (data not shown). To generate *Agpat6*$^{-/-}$ mice on an obese genetic background, *Agpat6*$^{+/-}$ mice were crossed with *Lep*$^{+/ob}$ (C57BL/6J background; obtained from Jackson Laboratory), and *Agpat6*$^{+/-}$ *Lep*$^{+/ob}$ offspring were intercrossed to produce *Agpat6*$^{-/-}$ *Lep*$^{ob/ob}$ animals. Because of the generation of greater numbers of female animals, analysis was restricted to females.

Gene expression analyses

Total RNA was isolated from mouse tissues by extraction with TRIzol (Invitrogen, Carlsbad, CA). Two micrograms of RNA was reverse-transcribed with oligo(dT) and random primers (Invitrogen). Five percent of the resulting cDNA was used for each RT-PCR or real-time PCR. Real-time PCR was performed in triplicate with Quantitect SYBR Green PCR mix (Qiagen, Valencia, CA) in an iCycler Realtime Detection System (Bio-Rad, Hercules, CA) as described (19). Standard curves were constructed with four serial dilution points of control cDNA (100 ng–100 pg). Data presented were derived from starting quantity (SQ) values of each sample normalized by the square root of the product of values obtained for the housekeeping genes *Hprt* (for hypoxanthine phosphoribosyltransferase) and *Tbp* (for TATA box binding protein) (20). Primer sequences used in these studies have either been described previously (21,22) or are shown in Table 1.

Histology

Fresh tissues were fixed in 4% paraformaldehyde and then dehydrated, cleared, embedded in paraffin, sectioned at 4 μm, and stained with hematoxylin/eosin. For β-galactosidase staining, tissues were fixed and stained as described previously (23). For adipose size measurement, randomly selected sections from three wild-type mice and three *Agpat6*$^{-/-}$ mice were used. Sections were digitized, and cell surface area was quantified with NIH Image 1.62 (Wayne Rasband, National Institutes of Health). Cells from each treatment (n = 200) were analyzed to obtain a mean ± SD in arbitrary units.

Plasma glucose, leptin, and insulin

Glucose levels were determined with a One Touch Ultra Blood Glucose Monitor (Lifescan, Milpitas, CA). Insulin levels were determined with an ultrasensitive murine enzyme immunoassay (ALPCO Diagnostics, Windham, NH). Leptin levels were measured by immunoassay (R&D Systems, Minneapolis, MN). Measurements were made in duplicate samples according to the manufacturers' protocols.

Indirect calorimetry and core body temperature

Activity and oxygen consumption were determined with an Oxymax single cage system and recorded with Oxymax version 3.2 software (Columbus Instruments, Columbus, OH). Horizontal and vertical activity were determined with light beams positioned at 2 and 5 cm from the bottom of the cage to record distance walked by the mouse (cm/h) and rearing on hind legs (counts/h). Oxygen consumption and CO_2 production were recorded every 6 min throughout a 24 h period. Values were averaged over light (7 AM–6 PM) and dark (6 PM–7 AM) periods. Core body temperature was measured in all mice with a Ret-3 mouse rectal probe attached to a BAT-10 multipurpose digital thermometer (Physitemp Instruments, Clifton, NJ).

Lipid analysis

For tissue lipid analysis, samples were homogenized in 0.25 M sucrose, 20 mM Tris-Cl, pH 7.5, 5 mM EDTA, and 1 mM PMSF with a mechanical ultra-turrax (Janke & Kunkel, Cincinnati, OH). Total proteins were quantified for normalization between samples (BCA kit; Pierce, Rockford, IL), and triglycerides were measured with L-Type TG H reagents (Wako Pure Chemical Industries, Ltd., Richmond, VA) in homogenates or after Folch lipid extraction (24). Thin-layer chromatography was also performed on Folch lipid extracts. Briefly, tissue homogenates were extracted with chloroform-methanol (2:1, v/v). After vortexing and centrifugation, the organic phase was dried under N_2, lipids were resuspended in chloroform, and chromatography was performed on silica gel plates with a hexane-ethyl ether-acetic acid (80:20:1) solvent system. Lipids were visualized with iodine vapor and identified based on comigration with lipid standards. For quantitative analysis of the lipid metabolome, plasma and tissues (n = 3 for each group) in chow-fed mice were processed as described previously (25). Data are expressed as fold difference compared with the wild-type mice or percentage of the lipid class, as indicated in the text.

RESULTS

Expression patterns of eight *Agpat* genes

The *Agpat6* cDNA was initially cloned from human (known as LPAAT-ζ), and examination in a limited set of tissues showed highest expression in skeletal muscle (13). A reassessment of the tissue distribution of *Agpat6* mRNA in a larger set of mouse tissues by Northern blot revealed prominent expression in adipose tissue (brown adipose > white adipose) and liver, as well as in testis, with low expression in skeletal muscle (9). To further characterize the mRNA expression distribution of *Agpat6* and other family members, we performed real-time RT-PCR in several fat depots, liver, and brain from C57BL/6J mice. Figure 1 shows that among adipose tissue depots, *Agpat6* mRNA is expressed at highest levels in intrascapular brown adipose tissue (BAT), with high levels also detected in visceral white adipose tissue (WAT) depots (omental, epididymal, and retroperitoneal fat pads), and much lower levels were seen in subcutaneous (inguinal) fat tissue. Expression in liver was similar to that in visceral WAT, suggesting a function for AGPAT6 in tissues with important roles in triglyceride metabolism, including fat and liver. A similar expression analysis of the other putative *Agpat* genes revealed that BAT is also a major site of expression for *Agpat1*, *Agpat2*, *Agpat3*, and *Agpat7*. All of the genes except *Agpat4* and *Agpat7* exhibited substantial expression in WAT, with visceral depots being the major site for WAT expression for all genes except *Agpat5*, which showed highest expression in inguinal WAT. *Agpat4* had a distinct pattern, with expression mainly in brain, whereas the closest homolog of *Agpat6*, *Agpat8*, was restricted primarily to WAT, with no expression in brain or liver. These results show that the *Agpat* gene family members have distinct, but overlapping, gene expression patterns.

Generation of *Agpat6*$^{-/-}$ mice by gene-trap

To produce *Agpat6*$^{-/-}$ mice, we used an embryonic stem cell line carrying an insertional mutation in *Agpat6* (BayGenomics cell line DTM030). The insertion is located in intron 2 of *Agpat6* (which contains 13 exons and 12 introns) and results in the production of a fusion transcript containing the first two *Agpat6* exons joined in-frame to a *βgeo* reporter gene. The resulting fusion protein is expected to contain only the first 55 amino acids of AGPAT6, which would be reduced to 18 amino acids upon cleavage of the signal peptide (Fig. 2A). This deletion, therefore, eliminates most of the protein, including the conserved motifs implicated in catalysis (NHTSxxD) and glycerol-3-phosphate binding (PEGTC) (9,26).

ES cells carrying the *Agpat6* mutation were injected into mouse blastocysts, and chimeric offspring were bred to produce heterozygous *Agpat6* knockout mice. Homozygous mutant

mice were obtained at the predicted Mendelian frequency, indicating that the AGPAT6 protein is not required for survival. The absence of *Agpat6* mRNA in homozygous mice was confirmed by RT-PCR using primers in the 3′ portion of the transcript (Fig. 2B). Staining of BAT from *Agpat6*$^{-/-}$ mice for *lacZ* expression revealed a strong blue stain in BAT (Fig. 2C), in agreement with the gene expression data. To determine whether the expression of other members of the *Agpat* gene family was upregulated in response to AGPAT6 deficiency, we measured mRNA expression of *Agpat1–Agpat8* in BAT of the mutant mice. No significant differences in expression levels were observed between wild-type and *Agpat6*$^{-/-}$ mice (data not shown).

Agpat6$^{-/-}$ mice have reduced body weight and fat mass and are resistant to obesity

Based on its prominent expression in adipose tissue and its predicted role in triglyceride biosynthesis, we hypothesized that *Agpat6* deficiency might affect adipose tissue mass and body weight. Analysis of body weight in *Agpat6*$^{-/-}$ mice from weaning through 6 months of age revealed substantially lower body weight than in wild-type or *Agpat6*$^{+/-}$ mice (Fig. 3A). At 6 months of age, the *Agpat6*$^{-/-}$ mice showed a reduction of 10 g (~25%) in body weight. Analysis of the total carcasses of mice from which WAT and BAT depots had been removed showed a tendency toward a lower percentage of carcass fat in *Agpat6*$^{-/-}$ mice (12.0 ± 4.5% vs. 6.1 ± 2.7%), although this difference did not reach significance ($P = 0.065$, n = 4 in each group). To determine whether *Agpat6* deficiency confers resistance to obesity, wild-type and *Agpat6*$^{-/-}$ mice were fed a HF/HC diet for 15 weeks or crossed onto the genetically obese leptin-deficient *ob/ob* background. On both the HF/HC diet and the *ob/ob* background, *Agpat6*$^{-/-}$ mice maintained significantly lower body weight and did not become obese (Fig. 3B, C). Thus, *Agpat6* deficiency protects against both diet-induced obesity and genetically induced obesity.

To determine whether the reduced body weight in *Agpat6*$^{-/-}$ mice was attributable to decreased adipose tissue mass, we isolated gonadal and inguinal WAT and interscapular BAT fat pads. There was a significant decrease in the proportion of body weight composed of gonadal fat on both chow (1.7 ± 0.26% vs. 1.2 ± 0.14%; $P < 0.05$) and HF/HC (6.7 ± 2.1% vs. 4.6 ± 1.4%; $P < 0.05$) diets. These differences in fat mass were reflected in reduced leptin mRNA in adipose tissue and circulating leptin levels on both chow and high-fat diets (Fig. 3D). Although body weight was clearly reduced by *Agpat6* deficiency, no significant differences in percentage of fat mass were observed in wild-type and *Agpat6*$^{-/-}$ mice on the *ob/ob* background. *Agpat6*$^{-/-}$ mice exhibited no difference from wild-type mice in proportional liver weight on either chow or HF/HC diet or on the obese genetic background.

Subdermal lipodystrophy in *Agpat6*$^{-/-}$ mice

Histological examination of adipose tissue depots revealed major differences between wild-type and *Agpat6*$^{-/-}$ mice. First, we observed an absence of subdermal fat in the skin of *Agpat6*$^{-/-}$ mice that were older than 4 months of age (Fig. 4A). Staining for β-galactosidase expression in *Agpat6*$^{-/-}$ skin sections revealed substantial *Agpat6* expression in the subdermal layer (Fig. 4B). We did not observe changes in the thickness of the epidermis, in the number of fat cells surrounding the sebaceous glands, or in the cellular infiltration of the dermis in *Agpat6*$^{-/-}$ mice. However, lipid extraction of skin biopsies revealed a striking reduction in triglyceride content in *Agpat6*$^{-/-}$ mice (Fig. 4C). Analysis of neutral lipid species in skin by thin-layer chromatography confirmed a striking depletion of triglycerides, diacylglycerols (DAGs), and free fatty acids in *Agpat6*$^{-/-}$ lipid extracts, whereas cholesterol levels appeared normal (Fig. 4C). To determine whether lipid depletion in the skin affected the integrity and function of the fur coat, we assessed water repulsion with a swimming test (7). No differences were observed between wild-type and *Agpat6*$^{-/-}$ mice (data not shown). Thus, *Agpat6* deficiency leads to a subdermal lipodystrophy but does not appear to alter permeability functions of the fur.

The BAT and gonadal WAT depots in chow-fed *Agpat6*$^{-/-}$ mice also exhibited decreased triglyceride content (Fig. 5A, B). The difference in triglyceride content in BAT and WAT was not observed on the high-fat diet (Fig. 5B), suggesting the existence of a compensatory mechanism involving dietary lipids. On the *ob/ob* background, *Agpat6*$^{-/-}$ mice had reduced triglyceride levels in BAT but not in gonadal WAT (Fig. 5B). The average size of adipocytes in the gonadal fat was reduced in *Agpat6*$^{-/-}$ mice on both the chow and HF/HC diets (Fig. 5C).

Reduced fat mass and smaller adipocyte size are typically associated with insulin sensitivity. Although there were no significant differences in glucose levels in *Agpat6*$^{-/-}$ versus wild-type mice, a trend toward reduced insulin levels was observed in *Agpat6*$^{-/-}$ mice on the *ob/ob* background (Table 2). On the chow diet, *Agpat6*$^{-/-}$ mice had lower plasma triglyceride levels, but this decrease was not observed on the HF/HC diet or on the *ob/ob* background. Interestingly, the triglyceride content of the livers of *Agpat6*$^{-/-}$ mice on the *ob/ob* background was increased (1.3 ± 0.6 vs. 2.6 ± 0.5 μg/mg protein; $P < 0.05$), suggesting partial reallocation of dietary fat storage from adipose tissue to liver.

Altered fatty acid composition in lipids from BAT and liver of *Agpat6*$^{-/-}$ mice

A quantitative assessment of lipid composition and fatty acid distribution in plasma, BAT, and liver was generated with a combination of thin-layer and gas chromatography. Table 3 presents the concentrations of triacylglycerols (TAGs), DAGs, phospholipids, and the constituent fatty acids in each species. The data are expressed as relative levels in *Agpat6*$^{-/-}$ compared with wild-type mice. Fatty acid compositions of each lipid class expressed as mol% are reported in supplementary Table I and summarized below. No statistically significant differences were noted in the concentrations of lipid classes in the plasma. In BAT, there was a trend toward decreased TAG (311,003 ± 92,183 vs. 246,995 ± 25,011 nmol/g) and DAG (3,494 ± 751 vs. 2,232 ± 302 nmol/g) levels, although the differences did not achieve statistical significance, perhaps because of the small numbers of samples (n = 3 for each genotype). There were, however, significant alterations in MUFA versus PUFA composition in several lipid classes in the *Agpat6*$^{-/-}$ BAT. TAG had reduced MUFA (48.3% vs. 40.8%; $P < 0.05$); DAG showed a similar decrease in MUFA (38.0% vs. 33.8%) and a concomitant increase in PUFA (21.6% vs. 27.0%; $P < 0.05$). The phosphatidylcholine fraction also contained less MUFA and more PUFA, and the proportion of PUFA in free fatty acids was also increased (17.3% vs. 25.9%; $P < 0.05$), whereas saturated fatty acids (48.6% vs. 42.1%; $P < 0.05$) were reduced (see supplementary Table I).

The liver also exhibited a significant reduction in TAG concentration (161,521 ± 11,829 vs. 88,158 ± 7,532 nmol/g; $P < 0.05$) and an increase in lysophosphatidylcholine (1,110 ± 148 vs. 1,670 ± 245 nmol/g; $P < 0.05$). The reduction in TAG was characterized by a decrease in all classes of fatty acids (saturated, monounsaturated, and polyunsaturated), with a redistribution of MUFA (37.4 ± 0.5% vs. 33.8 ± 1.2%; $P < 0.05$) to PUFA (37.2 ± 0.5% vs. 40.3 ± 2.7%; $P < 0.05$). Overall, *Agpat6*$^{-/-}$ mice had reduced concentrations of TAG in the tissues and altered fatty acid composition, with reduced MUFA and increased PUFA contents.

Increased energy expenditure and normal thermogenesis in *Agpat6*$^{-/-}$ mice

The observed reduction in body weight and resistance to obesity in *Agpat6*$^{-/-}$ mice suggested altered food intake, activity, or energy metabolism. Food intake and activity were comparable to those of wild-type mice (Fig. 6A, B). However, *Agpat6*$^{-/-}$ mice showed higher energy expenditure by indirect calorimetry during both light (sleeping) and dark (active) periods of the diurnal cycle (Fig. 6C). No differences were observed in respiratory quotient (data not shown). Despite increased energy expenditure, core body temperature at room temperature was identical in wild-type and *Agpat6*$^{-/-}$ mice (36.3 ± 0.58C vs. 36.3 ± 0.4°C; n = 9). The maintenance of normal body temperature despite increased energy expenditure raises the

possibility that increased energy expenditure is an adaptation to maintain body temperature in the absence of a normal insulating layer of subdermal fat (Fig. 4).

One key mechanism for heat generation and energy dissipation in rodents is thermogenesis in BAT. However, given the prominent expression of *Agpat6* in BAT, we wondered whether thermogenesis in this tissue might be impaired in *Agpat6*$^{-/-}$ mice. To assess thermogenic capacity, mice were housed at 4°C for 4 h. Wild-type mice are able to maintain adequate body temperature under these conditions, largely through nonshivering thermogenesis in BAT. We found that *Agpat6*$^{-/-}$ mice maintained the same body temperature as wild-type mice during this acute cold exposure, indicating that cold-induced thermogenesis is not compromised (data not shown). In addition, the expression of key thermogenic response genes, including uncoupling protein-1 and peroxisome proliferator-activated receptor γ coactivator-1α, and genes involved in fatty acid oxidation, including acyl-CoA oxidase-1 and carnitine palmitoyltransferase-1b (see supplementary Fig. I), were normal in BAT from *Agpat6*$^{-/-}$ mice. Thus, despite the reduced stores of triglycerides in the BAT, *Agpat6*$^{-/-}$ mice have a normal thermogenic response to acute cold exposure.

DISCUSSION

The AGPAT family contains at least eight members, raising the question of redundancy in physiological function. One approach to investigate this question is to produce and characterize mouse strains lacking specific AGPAT proteins. Here, we used a mutant ES cell line from a gene-trap resource to generate a mouse strain lacking AGPAT6. An analysis of this model indicates that, despite its sequence similarity and partially overlapping tissue expression pattern with other family members, AGPAT6 plays a critical physiological role in the accumulation of triglyceride in WAT and BAT depots, particularly in the subdermal region. Furthermore, AGPAT6 is required for triglyceride production in mammary epithelium, rendering *Agpat6*$^{-/-}$ mice unable to nurse their offspring (9). These studies demonstrate that AGPAT6 has a nonredundant function within the AGPAT family.

The phenotype of *Agpat6*$^{-/-}$ mice is consistent with a role for this enzyme in triglyceride synthesis in BAT and WAT and exhibits similarities to the phenotype of *Dgat1*$^{-/-}$ mice. *Agpat6*$^{-/-}$ mice have reduced triglyceride content in both BAT and WAT and smaller adipocytes in the gonadal fat pad. Particularly striking was the nearly complete absence of subdermal adipose tissue in mature *Agpat6*$^{-/-}$ mice. This depot-specific lipodystrophy is a unique feature of these mice and suggests a specific role for *Agpat6* in the accumulation of triglycerides in subdermal adipocytes. Similar to the *Dgat1*$^{-/-}$ mouse, *Agpat6*$^{-/-}$ mice exhibit ~25% lower body weight than wild-type counterparts on both chow and HF/HC diets (27). Deficiency in either *Agpat6* or *Dgat1* also leads to increased energy expenditure, conferring resistance to diet-induced obesity (4). However, whereas *Dgat1*$^{+/-}$ mice on a high-fat diet had body weights intermediate between wild-type and knockout mice (27), we observed no phenotype in heterozygous *Agpat6*$^{+/-}$ mice on either chow or HF/HC diet or on the obese genetic background. Both *Agpat6*$^{-/-}$ and *Dgat1*$^{-/-}$ mice are resistant to genetically induced obesity, but the effects of genetic background are distinct. Thus, *Agpat6*$^{-/-}$ mice are resistant to obesity on the leptin-deficient *ob/ob* genetic background, whereas *Dgat1*$^{-/-}$ mice are resistant to obesity on the Agouti yellow background but not on the *ob/ob* background (5). A possible explanation for the lack of effect of *Dgat1* deficiency on the *ob/ob* background is that leptin deficiency leads to a compensatory increase in *Dgat2* expression, leading to normal levels of triglycerides in adipose tissue. There appears to be no such compensation in the setting of *Agpat6* deficiency.

The profound defect in subdermal adipose tissue accumulation in *Agpat6*$^{-/-}$ mice underscores a specific role for AGPAT6 in this fat depot. This aspect of the phenotype was not evident until

mice reached ~4 months of age, at which time the subdermal adipose accumulation in wild-type mice was obvious. To investigate whether *Agpat6* might have a role in the differentiation of adipocyte precursors to mature adipoctyes, we isolated embryonic fibroblasts from wild-type and *Agpat6*$^{-/-}$ embryos and differentiated them in culture with the addition of appropriate hormones and peroxisome proliferator-activated receptor γ ligand (19). *Agpat6*$^{-/-}$ fibroblasts were capable of normal differentiation in culture, as determined by the accumulation of Oil Red O-staining droplets (L. Vergnes, unpublished data), suggesting that the lack of subdermal adipose tissue in the mutant mice is most likely a consequence of impaired triglyceride synthesis in these particular cells. Other mouse models with reduced subdermal adipose tissue include transgenic mice overexpressing human apolipoprotein C-I in the skin (28), fatty acid transport protein-4-deficient mice (29), and *Dgat1*$^{-/-}$ and *Dgat2*$^{-/-}$ mice (7,8). In each of these models, there were abnormalities in skin structure and function in addition to the adipose content, such as dry skin, hair loss, epidermal hyperplasia/hyperkeratosis, and abnormal sebaceous gland function. In contrast, the *Agpat6*$^{-/-}$ mice had normal-appearing hair and epidermis and did not have impaired water repulsion, suggesting a very specific role for AGPAT6 in lipid accumulation within subdermal adipocytes without affecting other characteristics of the skin.

The resistance to obesity in *Agpat6*$^{-/-}$ mice is likely related both to a role for AGPAT6 in triglyceride accumulation in adipose tissue and to the increased energy expenditure observed in these mice. The mechanism underlying the increased energy expenditure is unknown, but it does not appear to be caused by increased activity; therefore, it probably has a metabolic basis. It is clear that *Agpat6* deficiency does not impair acute cold-induced thermogenesis, suggesting that the reduction in BAT triglyceride content is not sufficient to deplete fuel for thermogenesis. Thus, the increased metabolic rate in *Agpat6*$^{-/-}$ mice may not be a direct consequence of the absence of AGPAT6 but rather a compensatory response to maintain normal body temperature in the absence of a subdermal adipose tissue layer.

The function of each AGPAT enzyme is not well established. The activities of AGPAT1 and AGPAT2 in converting lysophosphatidic acid to phosphatidic acid are well documented, but the activities of the other members of the family remain unclear. The existence of at least eight enzymes in the AGPAT protein family raises questions about the specific role of each member. Several possibilities exist. If all members do possess AGPAT activity, it is possible that distinct physiological roles arise from their specific tissue distributions or from biochemical differences among the enzymes in transferring acyl groups of different chain lengths. Some support for this latter possibility comes from the observation that the fatty acid composition of glycerolipids and phospholipids was altered in tissues of *Agpat6*$^{-/-}$ mice. Overall, there was an increase in PUFA at the expense of MUFA in TAGs, DAGs, and phospholipids, suggesting that AGPAT6 has a preference for MUFA substrates. On the other hand, it is also conceivable that AGPAT6 may function at a different step in TAG synthesis, acting as another type of glycerolipid acyltransferase. The ultimate answer to the role that each AGPAT plays awaits both biochemical characterization of purified enzymes and physiological analysis through the derivation and analysis of additional genetic models of AGPAT deficiency.

Supplementary Material

Refer to Web version on PubMed Central for supplementary material.

Abbreviations

AGPAT	1-acylglycerol-3-phosphate *O*-acyltransferase
BAT	brown adipose tissue

DAG	Diacylglycerol
DGAT1	acyl-coenzyme A:diacylglycerol acyltransferase-1
GPAT	glycerol-3-phosphate acyltransferase
HF/HC	high-fat/high-carbohydrate
TAG	Triacylglycerol
WAT	white adipose tissue

Acknowledgments

The authors thank Robert Chin and Ping Xu for mouse colony management and technical assistance. This work was supported by the National Institutes of Health National Heart, Lung, and Blood Institute Program for Genomic Applications (Grant U01 HL-66621).

REFERENCES

1. Agarwal AK, Garg A. Congenital generalized lipodystrophy: significance of triglyceride biosynthetic pathways. Trends Endocrinol. Metab 2003;14:214–221. [PubMed: 12826327]
2. Coleman RA, Lee DP. Enzymes of triacylglycerol synthesis and their regulation. Prog. Lipid Res 2004;43:134–176. [PubMed: 14654091]
3. Hammond LE, Gallagher PA, Wang S, Hiller S, Kluckman KD, Posey-Marcos EL, Maeda N, Coleman RA. Mitochondrial glycerol-3-phosphate acyltransferase-deficient mice have reduced weight and liver triacylglycerol content and altered glycerolipid fatty acid composition. Mol. Cell. Biol 2002;22:8204–8214. [PubMed: 12417724]
4. Smith SJ, Cases S, Jensen DR, Chen HC, Sande E, Tow B, Sanan DA, Raber J, Eckel RH, Farese RV Jr. Obesity resistance and multiple mechanisms of triglyceride synthesis in mice lacking Dgat. Nature 2000;25:87–90.
5. Chen HC, Smith SJ, Ladha Z, RJensen D, Ferreira LD, Pulawa LK, McGuire JG, Pitas RE, Eckel RH, Farese RV Jr. Increased insulin and leptin sensitivity in mice lacking acyl CoA:diacylglycerol acyltransferase 1. J. Clin. Invest 2002;109:1049–1055. [PubMed: 11956242]
6. Chen HC, Ladha Z, Smith SJ, Farese RV Jr. Analysis of energy expenditure at different ambient temperatures in mice lacking DGAT1. Am. J. Physiol. Endocrinol. Metab 2003;284:E213–E218. [PubMed: 12388146]
7. Chen HC, Smith SJ, Tow B, Elias PM, Farese RV Jr. Leptin modulates the effects of acyl CoA:diacylglycerol acyltransferase deficiency on murine fur and sebaceous glands. J. Clin. Invest 2002;109:175–181. [PubMed: 11805129]
8. Stone SJ, Myers H, Brown BE, Watkins SM, Feingold KR, Elias PM, Farese RV Jr. Lipopenia and skin barrier abnormalities in DGAT2-deficient mice. J. Biol. Chem 2004;279:11767–11776. [PubMed: 14668353]
9. Beigneux AP, Vergnes L, Qiao X, Quatela S, Davis R, Watkins SM, Coleman RA, Walzem RL, Philips M, Reue K, Young S. Agpat6—a novel lipid biosynthetic gene required for triacylglycerol production in mammary epithelium. J. Lipid Res 2006;47:734–744. [PubMed: 16449762]
10. Aguado B, Campbell RD. Characterization of a human lysophosphatidic acid acyltransferase that is encoded by a gene located in the class III region of the human major histocompatibility complex. J. Biol. Chem 1998;273:4096–4105. [PubMed: 9461603]
11. Eberhardt C, Gray PW, Tjoelker LW. Human lysophosphatidic acid acyltransferase. cDNA cloning, expression, and localization to chromosome 9q34.3. J. Biol. Chem 1997;272:20299–20305. [PubMed: 9242711]
12. Kawaji H, Schonbach C, Matsuo Y, Kawai J, Okazaki Y, Hayashizaki Y, Matsuda H. Exploration of novel motifs derived from mouse cDNA sequences. Genome Res 2002;12:367–378. [PubMed: 11875024]

13. Li D, Yu L, Wu H, Shan Y, Guo J, Dang Y, Wei Y, Zhao S. Cloning and identification of the human LPAAT-zeta gene, a novel member of the lysophosphatidic acid acyltransferase family. J. Hum. Genet 2003;48:438–442. [PubMed: 12938015]

14. Ye GM, Chen C, Huang S, Han DD, Guo JH, Wan B, Yu L. Cloning and characterization a novel human 1-acyl-snglycerol-3-phosphate acyltransferase gene AGPAT7. DNA Seq 2005;16:386–390. [PubMed: 16243729]

15. Lu B, Jiang YJ, Zhou Y, Xu FY, Hatch GM, Choy PC. Cloning and characterization of murine 1-acyl-sn-glycerol 3-phosphate acyltransferases and their regulation by PPARalpha in murine heart. Biochem. J 2005;385:469–477. [PubMed: 15367102]

16. Agarwal AK, Arioglu E, De Almeida S, Akkoc N, Taylor SI, Bowcock AM, Barnes RI, Garg A. AGPAT2 is mutated in congenital generalized lipodystrophy linked to chromosome 9q34. Nat. Genet 2002;31:21–23. [PubMed: 11967537]

17. Magre J, Delepine M, Van Maldergem L, Robert JJ, Maassen JA, Meier M, Panz VR, Kim CA, Tubiana-Rufi N, Czernichow P, et al. Prevalence of mutations in AGPAT2 among human lipodystrophies. Diabetes 2003;52:1573–1578. [PubMed: 12765973]

18. Stryke D, Kawamoto M, Huang CC, Johns SJ, King LA, Harper CA, Meng EC, Lee RE, Yee A, L'Italien L, et al. BayGenomics: a resource of insertional mutations in mouse embryonic stem cells. Nucleic Acids Res 2003;31:278–281. [PubMed: 12520002]

19. Phan J, Peterfy M, Reue K. Lipin expression preceding peroxisome proliferator-activated receptor-gamma is critical for adipogenesis in vivo and in vitro. J. Biol. Chem 2004;279:29558–29564. [PubMed: 15123608]

20. Vandesompele J, De Preter K, Pattyn F, Poppe B, Van Roy N, De Paepe A, Speleman F. Accurate normalization of realtime quantitative RT-PCR data by geometric averaging of multiple internal control genes. Genome Biol 2002;3:0034.1–0034.11.

21. Phan J, Reue K. Lipin, a lipodystrophy and obesity gene. Cell Metab 2005;1:73–83. [PubMed: 16054046]

22. Peterfy M, Phan J, Reue K. Alternatively spliced lipin isoforms exhibit distinct expression pattern, subcellular localization, and role in adipogenesis. J. Biol. Chem 2005;280:32883–32889. [PubMed: 16049017]

23. Beigneux AP, Kosinski C, Gavino B, Horton JD, Skarnes WC, Young SG. ATP-citrate lyase deficiency in the mouse. J. Biol. Chem 2004;279:9557–9564. [PubMed: 14662765]

24. Folch J, Lees M, Sloane Stanley GH. A simple method for the isolation and purification of total lipides from animal tissues. J. Biol. Chem 1957;226:497–509. [PubMed: 13428781]

25. Watkins SM, Lin TY, Davis RM, Ching JR, DePeters EJ, Halpern GM, Walzem RL, German JB. Unique phospholipid metabolism in mouse heart in response to dietary docosahexaenoic or alpha-linolenic acids. Lipids 2001;36:247–254. [PubMed: 11337979]

26. Leung DW. The structure and functions of human lysophosphatidic acid acyltransferases. Front. Biosci 2001;6:D944–D953. [PubMed: 11487472]

27. Chen HC, Farese RV Jr. Inhibition of triglyceride synthesis as a treatment strategy for obesity: lessons from DGAT1-deficient mice. Arterioscler. Thromb. Vasc. Biol 2005;25:482–486. [PubMed: 15569818]

28. Jong MC, Gijbels MJJ, Dahlmans VEH, van Gorp PJJ, Koopman S-J, Ponec M, Hofker MH, Havekes LM. Hyperlipidemia and cutaneous abnormalities in transgenic mice over-expressing human apolipoprotein C1. J. Clin. Invest 1998;101:145–152. [PubMed: 9421476]

29. Herrmann T, van der Hoeven F, Grone H-J, Stewart AF, Langbein L, Kaiser I, Liebisch G, Gosch I, Buchkremer F, Drobnik W, et al. Mice with targeted disruption of the fatty acid transport protein 4 (Fatp4, Slc274a) gene show features of lethal restrictive dermopathy. J. Cell Biol 2003;161:1105–1115. [PubMed: 12821645]

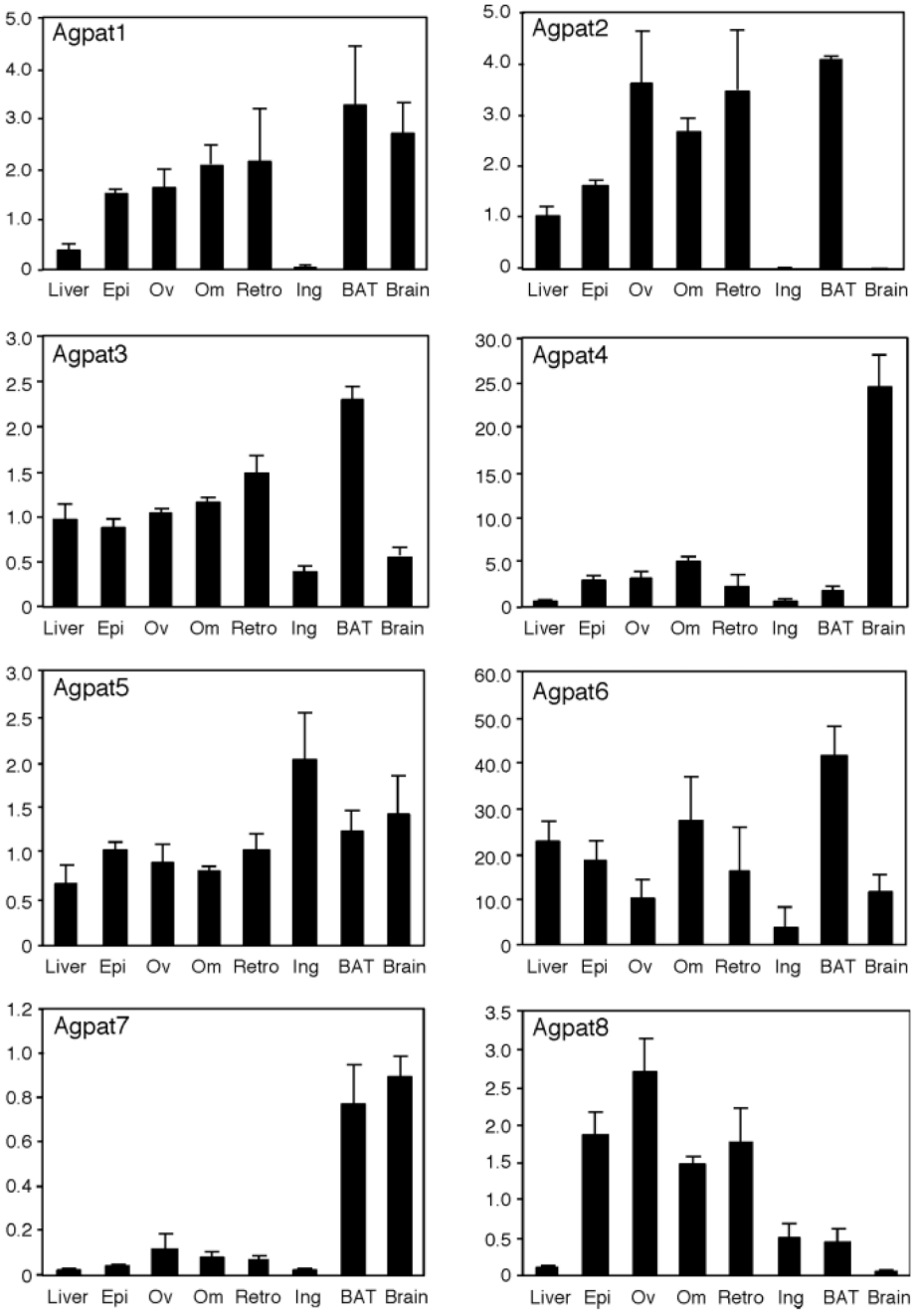

Fig. 1.

mRNA levels of 1-acylglycerol-3-phosphate *O*-acyltransferase (AGPAT)-related enzymes in different tissues. Data were obtained by real-time PCR from three individual C57BL/6J mice. Values shown represent means ± SD in arbitrary units, normalized as described in Materials and Methods. Epi, epididymal fat; Ov, ovarian fat; Om, omental fat; Retro, retroperitoneal fat; Ing, inguinal fat; BAT, brown adipose tissue.

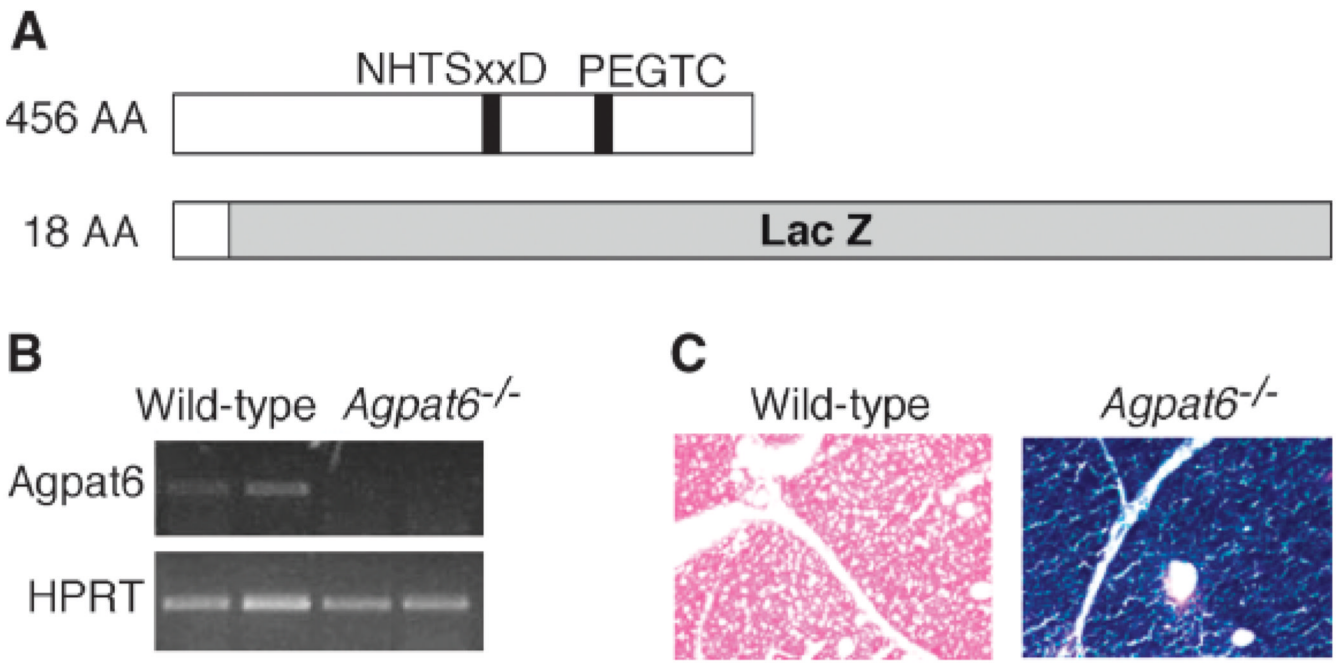

Fig. 2.

Generation of *Agpat6*-deficient (*Agpat6*$^{-/-}$) mice. A: Scheme representing the wild-type protein and the AGPAT6$^{-/-}$ fusion protein generated from the gene-trap allele. The size of the AGPAT6 protein portion in amino acids (AA) is noted at left. NHTxxD and PEGTC indicate the putative catalytic and glycerol-3-phosphate binding domains, respectively. B: RT-PCR showing the absence of normal AGPAT6 mRNA in *Agpat6*$^{-/-}$ mice. Primers used to amplify AGPAT6 cDNA were localized downstream of the gene-trap vector insertion site. HPRT, hypoxanthine phosphoribosyltransferase. C: β-Galactosidase staining of a BAT section. The AGPAT6-βgeo fusion protein shows strong staining throughout the BAT. Magnification, 20×.

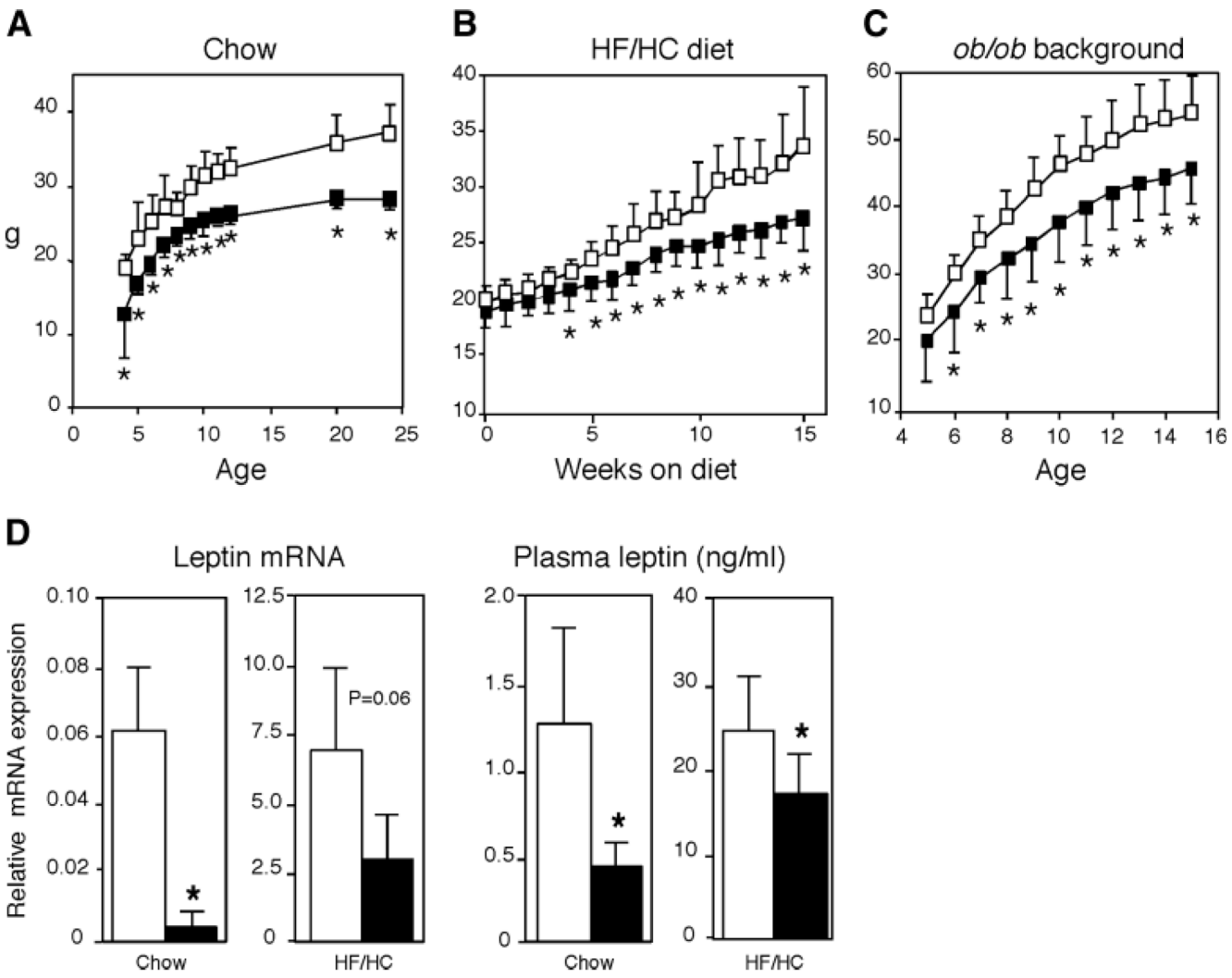

Fig. 3.

Body weight curves and leptin levels in wild-type and *Agpat6*$^{-/-}$ mice. A: Male mice fed a chow diet from birth to 25 weeks of age. Chow-fed female mice were not analyzed at all time points but exhibited a similar significant difference in body weight compared with wild-type mice at 6 months of age (data not shown). B: Female mice fed a high-fat/high-carbohydrate (HF/HC) diet for 15 weeks beginning at 8 weeks of age. Male mice were not analyzed. C: Female mice on an *ob/ob* background from 5 to 15 weeks of age. Male mice were not analyzed. For A–C, open and closed squares represent wild-type and *Agpat6*$^{-/-}$ mice, respectively (n = 8 in each group). D: The left panels represent leptin mRNA levels in gonadal fat tissue determined by real-time PCR (n = 4 for each group). The right panels show plasma leptin levels obtained by ELISA. Open and closed bars represent wild-type and *Agpat6*$^{-/-}$ mice, respectively. Chow-fed values were from the male mice shown in A and used epididymal fat tissue; HF/HC values were from female mice shown in B and used periuterine fat tissue. * $P < 0.05$.

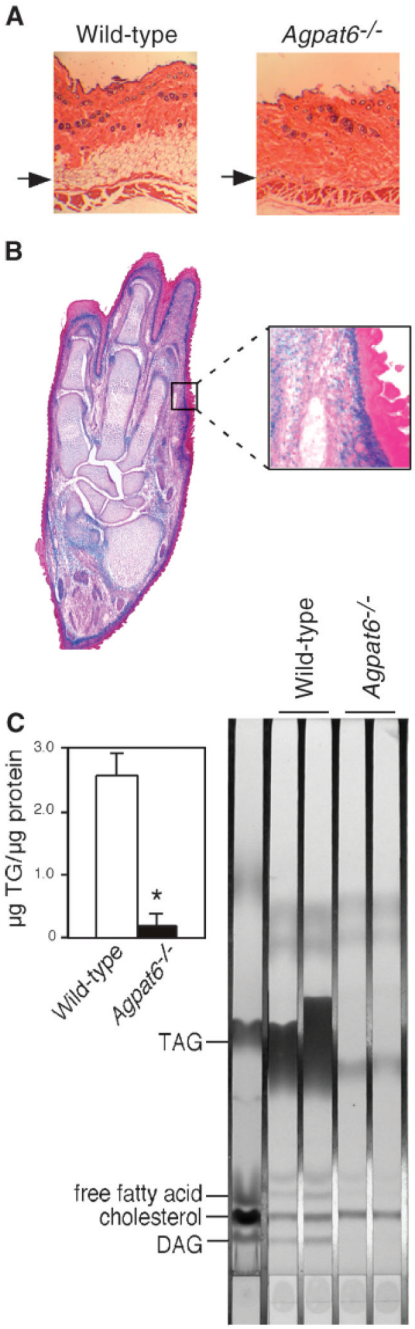

Fig. 4.

Subdermal adipose tissue deficiency in the *Agpat6*$^{-/-}$ mouse. A: Skin cross-sections with hematoxylin/eosin. Arrows indicate the presence of the fat cell layer in wild-type mice but not in *Agpat6*$^{-/-}$ mice. Magnification, 160×. B: Left, β-galactosidase staining of a paw cross-section from an *Agpat6*$^{-/-}$ mouse showing AGPAT expression in the subdermal layer. Magnification, 40×. Right, close-up of the boxed region at left. Magnification, 100×. C: Triglyceride (TG) levels (left) and neutral lipid species determined by thin-layer chromatography (right) from skin lipid extracts of chow-fed mice. DAG, diacylglycerol; TAG, triacylglycerol. * $P < 0.001$.

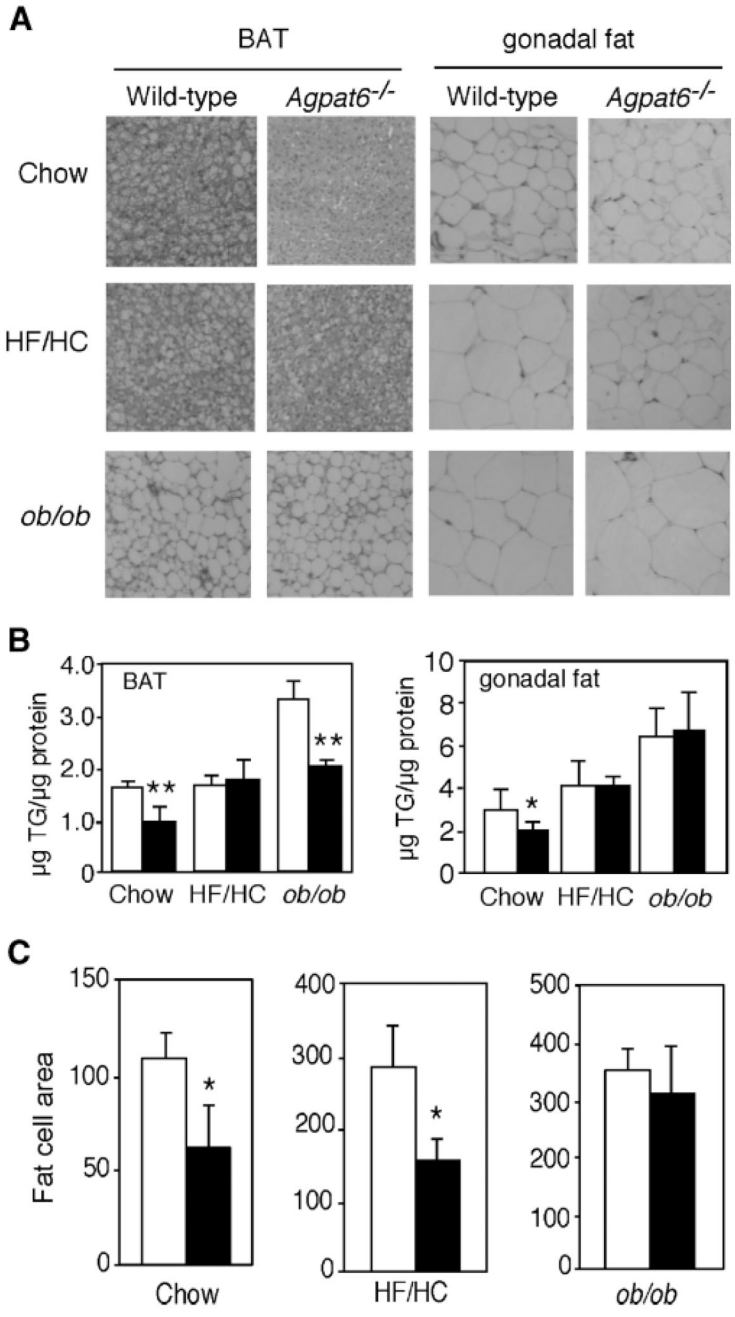

Fig. 5.

Altered fat cell size and triglyceride content in *Agpat6*$^{-/-}$ tissues. A: Hematoxylin/eosin-stained BAT and gonadal fat pad sections from mice fed chow, fed a HF/HC diet, or on the *ob/ob* background, as indicated. Magnification, 320×. B: Triglyceride (TG) levels in BAT and gonadal fat tissue isolated from mice under the conditions shown in A. C: Quantitation of fat cell area in gonadal fat pad sections from female mice under the conditions indicated. Randomly chosen sections from three wild-type mice and three *Agpat6*$^{-/-}$ mice were used, and a total of 200 cells from each were measured with NIH Image software. Values are expressed as means ± SD in arbitrary units. Open and closed bars represent wild-type and *Agpat6*$^{-/-}$ mice, respectively. * $P < 0.05$, ** $P < 0.01$.

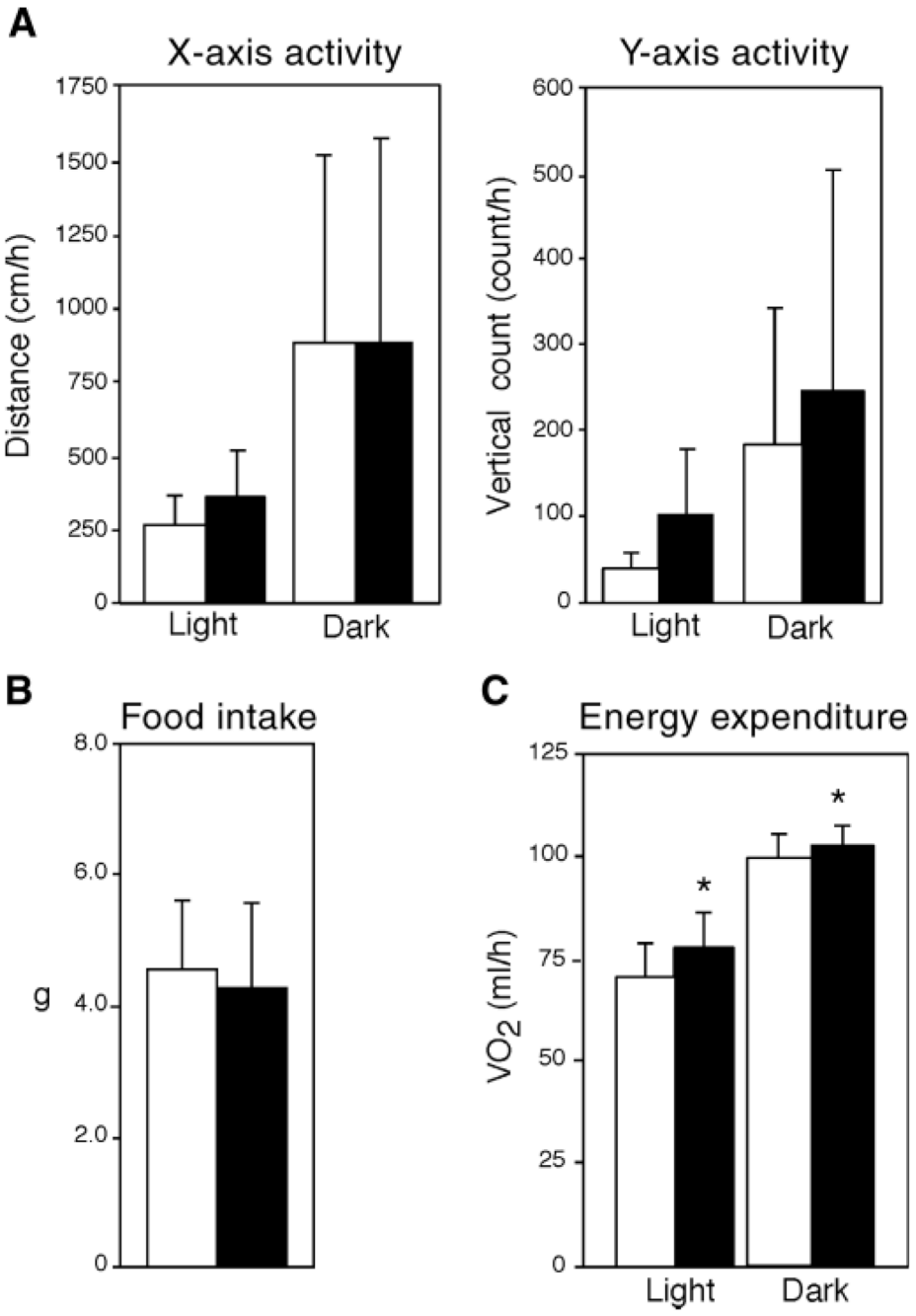

Fig. 6.

Increased energy expenditure in *Agpat6*$^{-/-}$ mice. A: Activity measurements in chow-fed mice. The left panel represents the distance covered per hour, and the right panel represents vertical rearing activity. The light period was from 7 AM to 6 PM, and the dark period was from 6 PM to 7 AM (n = 6 mice for each group). B: Average daily food consumption determined on four independent days for each mouse (n = 8 mice for each group). C: Oxygen consumption (VO_2, ml/h) determined by indirect calorimetry (n = 8 mice for each group). Open and closed bars represent wild-type and *Agpat6*$^{-/-}$ mice, respectively. * $P < 0.01$.

TABLE 1

Primer sequences used in real-time PCR experiments

Gene	Forward	Reverse
Agpat1	cacccaggatgtgagagtctg	ctgacaacgtccaggcgagg
Agpat2	gcaacgacaatggggacctg	acagcatccagcacttgtacc
Agpat3	ctttaccacggcagtccagtg	tgcttgtacatctcttgcaggg
Agpat4	ccagcctcaaacaccacctg	gagcacttgtcctcatcctcc
Agpat5	agctgcagagctatgtgaacg	tcaaaagcaacgtgagtggcc
Agpat6	ggcagaggagctggagtc	tgttgtggtacgtaatgatgg
Agpat7	gacagtggctggtgccttcag	ctttgtacagcagccggtcag
Agpat8 (GenBank accession number NM_172715)	gtacatgcctcccatgactag	gatccgttgcccacgatcatc
Peroxisome proliferators-activated receptor γ coactivator-1α	ctgcgggatgatggagacag	cgttcgacctgcgtaaagt

Agpat, 1-acylglycerol-3-phosphate *O*-acyltransferase.

TABLE 2

Plasma levels of glucose, insulin, and triglycerides

Sex	Genotype	Condition	Glucose	Insulin	Triglycerides
			mg/dl	***μg/dl***	***mg/dl***
Male	Wild type	Chow diet	89 ± 16	0.14 ± 0.05	40 ± 19
Male	*Agpat6*$^{-/-}$	Chow diet	83 ± 18	0.12 ± 0.03	19 ± 9[a]
Female	Wild type	HF/HC diet	80 ± 17	0.38 ± 027	38 ± 20
Female	*Agpat6*$^{-/-}$	HF/HC diet	68 ± 15	0.34 ± 0.24	27 ± 9
Female	Wild type	*ob/ob* background	121 ± 46	7.40 ± 3.79	42 ± 22
Female	*Agpat6*$^{-/-}$	*ob/ob* background	170 ± 114	4.02 ± 0.82	44 ± 30

HF/HC, high-fat/high-carbohydrate.

[a] $P < 0.05$ versus the wild type.

TABLE 3

Effect of *Agpat6* deficiency on lipid composition in plasma, BAT, and liver

Tissue	Lipid class	Class	SFA	MUFA	PUFA	n3	n6	n7	n9	Plasmalogen lipids
Plasma	DAG	0.87	0.90	0.99	0.72	0.95	0.69	0.94	0.96	0.71
Plasma	TAG	0.71	0.73	0.61	0.77	0.84	0.75	0.59	0.62	0.67
Plasma	FFA	1.20	1.24	1.16	1.21	1.11	1.22	1.49	1.07	1.70
Plasma	LysoPC	0.97	0.99	0.89	0.95	1.20	0.92	0.99	0.87	1.10
Plasma	PC	1.09	1.08	0.94	1.15	1.32	1.12	1.05	0.91	1.21
Plasma	PE	1.23	1.27	1.14	1.23	1.19	1.24	1.96	0.99	1.05
BAT	DAG	0.64^{a}	0.63	0.57^{b}	0.80	0.31^{b}	0.91	0.48^{a}	0.60^{b}	0.34^{b}
BAT	TAG	0.79	0.86	0.67	0.97	0.63	1.00	0.68	0.67	0.59
BAT	FFA	0.79	0.70	0.74	1.15	0.62	1.23	0.55	0.78	N.D.
BAT	PC	1.07	1.07	0.76	0.19	1.07	1.23	0.71	0.76	0.88
Liver	DAG	0.68	0.69	0.61	0.74	0.77	0.74	0.58	0.62	0.57
Liver	TAG	0.55^{b}	0.56^{b}	0.49^{b}	0.59^{b}	0.61^{b}	0.59^{b}	0.47^{b}	0.50	0.04
Liver	FFA	1.17	1.47^{b}	0.76^{a}	1.18	1.32	1.16	0.79	0.75	4.65
Liver	LysoPC	1.50^{b}	1.57^{b}	1.49	1.38^{b}	1.14	1.47^{a}	0.68^{a}	1.70	0.56
Liver	PC	1.12	1.13	0.94	1.17^{b}	1.37^{b}	1.11^{a}	1.09	0.91	1.16
Liver	PE	1.05	1.07	0.99	1.05	1.20	0.98	1.05	0.97	1.28^{b}
Liver	PS	1.35	1.39	1.26	1.31	1.34	1.29	1.26	1.26	1.41

BAT, brown adipose tissue; DAG, diacylglycerol; N.D., not detectable; PC, phosphatidylcholine; PE, phosphatidylethanolamine; PS, phosphatidylserine; SFA, saturated fatty acid; TAG, triacylglycerol. Values represent the ratio of mean values from *Agpat6*$^{-/-}$ mice compared with wild-type mice (n = 3 for each) for total lipid class and the fatty acid constituents. Class and ratio of mass for lipid class are indicated; n3, n6, n7, and n9 represent positions of the double bond in the fatty acid chain.

$^{a}P < 0.08$ for *Agpat6*$^{-/-}$ versus the wild type.

$^{b}P < 0.05$ for *Agpat6*$^{-/-}$ versus the wild type.